MNRAS **000**, 1–14 (2015) Preprint 29 February 2016 Compiled using MNRAS LATEX style file v3.0

Resolving phase ambiguities in the calibration of redundant interferometric arrays: implications for array design

Binoy G. Kurien,[1,2]⋆ Vahid Tarokh,[1] Yaron Rachlin,[2] Vinay N. Shah,[2] Jonathan B. Ashcom[2]

[1]*Harvard Paulson School of Engineering and Applied Sciences, 29 Oxford St., Cambridge, MA, 02138*
[2]*MIT Lincoln Laboratory, 244 Wood St., Lexington, MA 02421*

Accepted XXX. Received YYY; in original form ZZZ

ABSTRACT

We provide new results enabling robust interferometric image reconstruction in the presence of unknown aperture piston variation via the technique of Redundant Spacing Calibration (RSC). The RSC technique uses redundant measurements of the same interferometric baseline with different pairs of apertures to reveal the piston variation among these pairs. In both optical and radio interferometry, the presence of phase wrapping in the measurements is a fundamental issue that needs to be addressed for reliable image reconstruction. In this paper, we show that these ambiguities affect recently-developed RSC phasor-based reconstruction approaches operating on the complex visibilities, as well as traditional phase-based approaches operating on their logarithm. We also derive new sufficient conditions for an interferometric array to be immune to these phase-wrap ambiguities in the sense that their effect can be rendered benign in image reconstruction. We show the implications of this property of *wrap-invariance* for imaging via phase closures and extend existing results involving the classical three-baseline closures to generalized closures. Furthermore we show that this property is conferred upon arrays whose interferometric graph satisfies a certain cycle-free condition. We specify this condition and, for cases in which this condition is not satisfied, we provide a simple algorithm for identifying those graph cycles which prevent its satisfaction. We apply this algorithm to diagnose and correct a member of a pattern family popular in the literature. **Finally, we show that wrap-invariance is a fundamental property which is important in certifying reliability of powerful existing RSC techniques in the literature.**

Key words: techniques: interferometric – techniques: image processing – atmospheric effects – methods: analytical – methods: numerical

1 INTRODUCTION

Optical interferometry is a multi-aperture imaging technique which is attracting increasing interest in the astronomical and remote-sensing communities. The appeal of this technique is primarily due to the high resolution it affords relative to single-aperture imaging. Namely, the angular resolution of a single aperture is limited by diffraction to $\frac{\lambda}{D}$, where λ is the wavelength of the light, and D is the diameter of the aperture. On the other hand, the achievable angular resolution of an interferometer is instead given by $\frac{\lambda}{B_{max}}$, where B_{max} is the maximum spatial separation of any two telescopes in the array. Therefore with interferometry one can achieve the same high resolution offered by an extremely large (and often prohibitively-costly) telescope by interfering light from several telescopes of practical size. Optical interferometers image a scene by sampling the 2D Fourier Transform of the scene. Several excellent surveys exist which describe the concept of interferometry, including Labeyrie et al. (2006), Glindemann (2011). Each pair of telescopes measures a single angular spatial frequency of $\frac{2\pi \boldsymbol{b}}{\lambda}$ radians, where $\boldsymbol{b}$ is the vector difference of the telescope positions, which is known as a *baseline*. For an array of N apertures, the data set then consists of all $\binom{N}{2}$ such measurements.

A principal challenge in interferometry is variation in the complex gains among the multiple apertures of the interferometer. In radio interferometry, this variation can arise from differences among the analog components of the antenna elements (e.g. cable length differences) in the array. In optical interferometry, atmospheric turbulence distorts

⋆ Email: bkurien@ll.mit.edu

the wavefronts arriving at each telescope aperture so that their effective path lengths from the target (or *optical pistons*) are altered by a random, non-uniform amount. For simplicity, we will heretofore refer to such aperture-specific phase variation as *optical path difference* (OPD), regardless of its source. As a result of OPD, the Fourier component measured by apertures i and j is given by $y_{ij} = |y_{ij}|e^{j\tilde{\theta}_{ij}}$, in which $\tilde{\theta}_{ij} = (\theta_{ij} + \delta\phi_{ij}) \mod 2\pi$ [1], and θ_{ij} is the true Fourier phase at spatial frequency $\frac{\boldsymbol{b}_{ij}}{\lambda}$, and $\delta\phi_{ij}$ represents the OPD observed between apertures i and j. One approach to eliminate OPD is to form triple products of the Fourier components along the sides of a baseline triangle (e.g. $\boldsymbol{b}_{12}$, $\boldsymbol{b}_{23}$, and $\boldsymbol{b}_{31}$). Note that the OPD cancels in these products and hence, like the Fourier magnitudes, these so-called *bispectra* are OPD-invariant observables. However, for a non-redundant array with $\binom{N}{2}$ distinct baselines, recovery of the Fourier phases from the bispectra phases is an ill-posed problem since there are only $\binom{N-1}{2}$ independent bispectra (Readhead et al. 1988). Successful bispectra-based image reconstruction remains feasible in spite of this ill-posedness (see e.g. Thiébaut (2013), Besnerais et al. (2008)), but in this case prior constraints (e.g. on the image support) must be enforced to regularize the reconstruction.

An alternative and intrinsically well-posed approach to prior-regularized reconstruction is to use baseline redundancy to explicitly solve for OPD variation; an array with baseline redundancy contains repeated instances of the same baseline involving distinct aperture pairs. Since Fourier phases can be assumed to be equal for all repeated baselines, an observed difference amongst their corresponding measurements exposes the contribution of the OPD. This idea of using redundant arrays to calibrate out OPD variation, known as *redundant spacing calibration (RSC)*, was developed in works such as those by Arnot et al. (1985) and Greenaway (1990). In recent years, innovation in optical technology has engendered a revival of interest in the RSC technique. The simultaneous (or *Fizeau*-style) measurement of fringes on a common focal plane has long been a popular method of acquiring many baseline measurements in an economical manner. However, the Fizeau method had been incompatible with RSC techniques since the fringes formed by each set redundant baselines would alias on the focal plane. An elegant solution to this problem was proposed by Perrin et al. (2006). This work developed the idea of segmenting the entrance pupil of a single telescope into an RSC arrangement of sub-pupils from which the light was then coupled via single mode fiber to a non-redundant exit pupil, thereby permitting unambiguous and simultaneous fringe detection for an RSC array. A reconstruction algorithm for this architecture was then proposed in Lacour et al. (2007). Even more recently, RSC has been implemented as the calibration scheme of choice for several radio interferometers: the Donald C. Backer Precision Array for Probing the Epoch of Reionization (PAPER) in South Africa (see Ali et al. (2015)), the MIT Epoch of Reionization (MITeOR) in the United States (see Zheng et al. (2014)), and the Ooty Radio Telescope (ORT) in India (see Marthi & Chengalur (2014)).

As will be shown below, $N-3$ independent redundant relations are required for unique determination of atmosphere and Fourier phases - a condition we will refer to as *critical redundancy*. An oft-cited drawback of the RSC approach is that it reduces the number of unique spatial frequencies measured by the interferometer. However, as Figure 1 illustrates, the fraction of distinct uv-samples sacrificed for critical redundancy becomes increasingly negligible as the number of apertures in the array increases. Nevertheless the RSC technique presents other challenges which must be overcome for reliable imaging. Central among these challenges is the problem of integer phase ambiguities which arise from the fact that the interferometric phase is only known modulo 2π. **Indeed these ambiguities have been shown to play an important role in accurately recovering sensor complex gains and object complex visibilities while imaging with real interferometric instruments (see e.g. Liu et al. (2014), Eastwood et al. (2009)).** In this paper, we describe these ambiguities and how they can be mitigated using a combination of lattice theory algorithms and careful array design. We will see that these ambiguities have a fundamental presence; namely, they exist whether the calibration strategy works with complex visibilities (which we call the *Phasor* approach) directly, or their respective logarithms (which we call the *Phase* approach). **To the best of our knowledge, the results in this paper are the first to provide array conditions allowing unambiguous interferometric phase determination in spite of wrap ambiguities in the Phase approach, and corresponding false minima in the objective of the Phasor approach.**

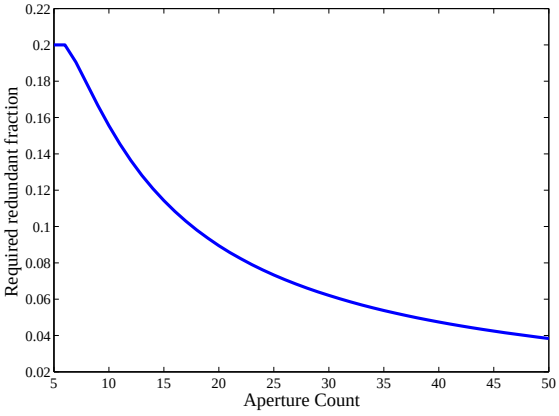

Figure 1. Fraction of redundant baselines required for critical redundancy vs. aperture count

To motivate the analysis in the paper, we provide an example illustrating the effect that wrap ambiguities can have in RSC-based image reconstruction. Consider the pattern depicted in the Figure 2. This pattern belongs to one of the more popular array classes in the interferometry literature: the so-called *Y-patterns* (see e.g. Arnot et al. (1985), Blanchard et al. (1996), Labeyrie et al. (2006), Eastwood et al. (2009), Liu et al. (2014)). The corresponding spatial, or *UV*, sampling is provided in the right panel of the Figure.

To demonstrate the potential effect of wrap

[1] In this paper, we use mod to denote the modulo operation

Figure 2. Y-pattern Array Example

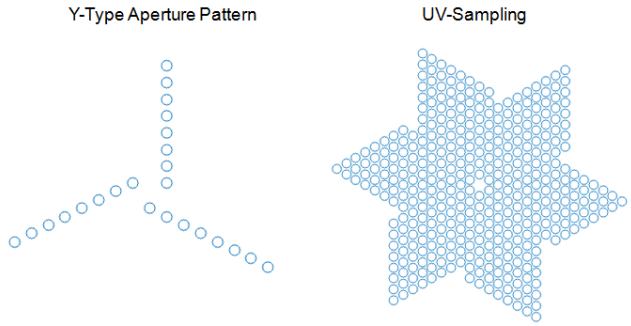

Figure 3. Reconstruction Results for Y-Pattern Example

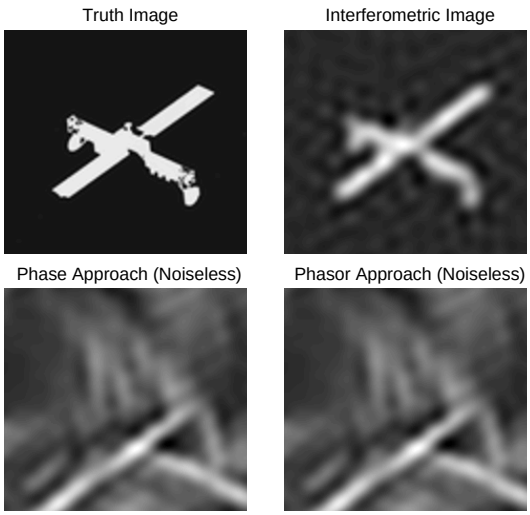

ambiguities on reconstruction, we simulated both Phase- and Phasor-based reconstruction from noiseless measurements with this pattern. The results are shown in Figure 3. The upper left panel shows the true image, and the upper right panel shows the **inverse Fourier transform of the UV-sampled visibility function of the object (i.e. the so-called *dirty*, or *interferometric* image)**. The lower left panel shows the reconstruction result with an implementation of the Phase method similar to that developed by Lannes (2003), and the lower right panel shows the same for an implementation of the Phasor method (Marthi & Chengalur 2014) (Lacour et al. 2007). Reconstruction suffers from phase wrapping error in the former case, and a corresponding false-minimum trap in the Phasor case. In the course of this paper, we will first identify this ambiguity from a mathematical perspective, relate it to a particular physical structure (i.e. the existence of a certain type of loop in the interferometric graph), and provide a simple algorithm for identifying such structures in an arbitrary array so that they can be remedied.

The paper is organized as follows. In Section II, we review previous work on the integer ambiguity problem, and discuss its presence in the Phase approach. **We provide new mathematical conditions for an aperture pattern to be *wrap-invariant*, meaning that the effect of the 2π-periodicity of the measured interferometric phase can be eliminated in image reconstruction.** These results are founded upon **techniques from lattice theory, as well as the** well-known Smith Normal Form (SNF) of an integer matrix. We show the implications of these results on imaging with three types of interferometric observables: the baseline phase measurements, their traditional closure phases, and generalized closure phases. In Section III, we relate these mathematical conditions to conditions on the aperture pattern itself. Namely we show that wrap-invariance is conferred upon arrays satisfying a certain loop-free condition. As an illustrative example, we diagnose a pattern belonging to the popular Y-pattern class and remedy it to be loop-free. Finally, in Section IV, we show that the computationally-complex SNF-based approach for ambiguity resolution is actually not necessary for wrap-invariance in many cases, as long as a **wrap-induced** image shift can be tolerated [2]. **For such scenarios, we show that wrap-invariance provides a certificate for the success of existing Phase and Phasor-based approaches in avoiding wrap-induced errors in the former, and false global minima in the latter.** Finally we summarize our results in Section V.

2 PHASE WRAPPING AMBIGUITIES IN RSC IMAGE RECONSTRUCTION

In this Section, we describe a Phase Approach algorithm leveraging the CVP-approach for phase-wrap resolution, which to the best of our knowledge was first developed in Lannes & Anterrieu (1999). We begin by identifying the fundamental phase ambiguity, and subsequently assess its impact on the phase error in the RSC phase solution. In the process, we develop mathematical conditions for wrap-invariance which will form the basis for the notion of a wrap-invariant pattern in Section 3. Finally, we assess our results in the context of similar results for approaches requiring the use of closure phases (Lannes 2003).

2.1 Identifying the Fundamental Phase Ambiguity

The traditional approach to RSC reconstruction operates on the measured baseline phases (see e.g. Arnot et al. (1985), Greenaway (1994)). To illustrate the approach, let us consider an interferometer which operates at a wavelength λ with two apertures (say, i and j) separated by a vector baseline distance of $\boldsymbol{b}_{ij}$. In the absence of any optical path difference, the interference pattern formed by these two apertures encodes a sample of the object's Fourier Transform at spatial frequency $\frac{\boldsymbol{b}_{ij}}{\lambda}$. Let the true Fourier phase (which we will refer to as *object phase*), measured by this interference pattern be denoted as θ_{ij}. The measured phase is given by:

$$\beta_{ij} = \theta_{ij} + \phi_j - \phi_i + 2\pi e \tag{1}$$

[2] **As will be shown, this image shift is distinct from the fundamental degeneracy of object position in interferometric measurements**

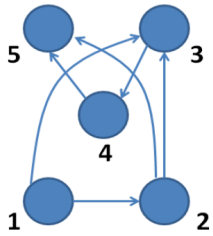

Figure 4. Example: 5-aperture RSC pattern. The six distinct baselines are shown.

where $\phi_j - \phi_i$ is the optical path difference between apertures j and i, and e is unknown phase wrap integer arising from the fact that interferometric phase measurements are only known modulo 2π.

Consider an interferometric array which simultaneously makes many such measurements amongst its N apertures. Suppose that of the array's $\binom{N}{2}$ baselines, d of them are distinct. Further suppose we have a solution set $\{\phi_i\}$ and $\{\theta_{ij}\}$ for these equations. Let $\boldsymbol{r}_i$ denote the vector position of the i-th aperture. As noted by several authors (see, e.g. Wieringa (1992)), we can obtain another valid solution set simply by replacing each ϕ_i with $\phi_i^p = \phi_i + \phi_0 + \boldsymbol{z} \cdot \boldsymbol{r}_i$, and each θ_{ij} with $\theta_{ij}^p = \theta_{ij} - \boldsymbol{z} \cdot (\boldsymbol{r}_j - \boldsymbol{r}_i)$, for arbitrary ϕ_0 and $\boldsymbol{z}$. Since the free vector $\boldsymbol{z}$ is a two-parameter vector representing the inherently-ambiguous position of the image within the Field-of-View and the free parameter ϕ_0 is simply a scalar piston offset, the kernel of the RSC system is three-dimensional. **This is the *tilt-position degeneracy* which is fundamental in interferometric reconstruction.** The end result is that the RSC system contains d unknown distinct object phases and N unknown aperture pistons, and is rank-deficient by at least 3. This implies that there are at most $(d + N - 3)$ linearly-independent equations in the RSC system, and hence at most $N - 3$ redundant relations can be linearly-independent. We will assume for the remainder of the paper that our array contains $N - 3$ independent relations. Under this assumption, we could in principle solve for a particular solution of this system by arbitrarily setting two object phases (whose spatial frequencies are not co-linear) and one piston phase. This particular solution would then differ from the true solution by a phase ramp in the Fourier domain, corresponding to an image shift in the spatial domain. **In this section we will instead construct a different particular solution which is immune to the effects of phase-wrapping by design**.

As an example, consider the simple array in Figure 4. There are $\binom{5}{2} = 10$ baselines, of which 4 are redundant. A critical array of 5 apertures would have 2 redundancies. Therefore this array possesses more redundancies than necessary (call it *strongly redundant*), and we anticipate that the resulting system will be overdetermined.

The measurement equations associated with this array can be written in matrix form:

$$\begin{bmatrix} 1 & 0 & 0 & 0 & 0 & 0 & 1 & -1 & 0 & 0 & 0 \\ 0 & 1 & 0 & 0 & 0 & 0 & 0 & 1 & -1 & 0 & 0 \\ 0 & 0 & 1 & 0 & 0 & 0 & 0 & 0 & 1 & -1 & 0 \\ 0 & 0 & 0 & 1 & 0 & 0 & 0 & 0 & 0 & 1 & -1 \\ 0 & 0 & 0 & 0 & 1 & 0 & 1 & 0 & -1 & 0 & 0 \\ 0 & 0 & 0 & 1 & 0 & 0 & 0 & 1 & 0 & -1 & 0 \\ 0 & 0 & -1 & 0 & 0 & 0 & 1 & 0 & 0 & -1 & 0 \\ -1 & 0 & 0 & 0 & 0 & 0 & 0 & 0 & 1 & 0 & -1 \\ 0 & 0 & 0 & 0 & 0 & 1 & 0 & 1 & 0 & 0 & -1 \\ 0 & 1 & 0 & 0 & 0 & 0 & 1 & 0 & 0 & 0 & -1 \end{bmatrix} \begin{bmatrix} \theta_{12} \\ \theta_{23} \\ \theta_{34} \\ \theta_{45} \\ \theta_{13} \\ \theta_{25} \\ \phi_1 \\ \phi_2 \\ \phi_3 \\ \phi_4 \\ \phi_5 \end{bmatrix} = \beta + 2\pi \boldsymbol{e} \tag{2}$$

Denoting the matrix above as $\mathbf{M}$, we can write such systems in compact form as:

$$\mathbf{M} \begin{bmatrix} \theta \\ \phi \end{bmatrix} = \beta + 2\pi \boldsymbol{e} \tag{3}$$

The example above illustrates that the general phase measurement matrix will have two sets of columns: one corresponding to the object phases, and one corresponding to the path differences. Adopting the notation of Lannes & Anterrieu (1999), let K denote the subspace spanned by the first set of columns, and L the subspace spanned by the second set.

If we let $n = \binom{N}{2}$ be the number of baselines in the array, the phase measurement matrix $\mathbf{M}$ will be of size $n \times (d + N)$. For a strongly-redundant array like the one in the example above, the column-space $K + L$ of the matrix will clearly not span $\mathbb{R}^n$. Therefore the wrapped measurement vector β will not in general fall in the the subspace $K + L$ (and potentially can be quite far from it). In the absence of measurement noise, we can unwrap these measurements by identifying those integer correction vectors $\boldsymbol{e}$ for which $\beta^* = \beta + 2\pi \boldsymbol{e}$ lies in $K + L$. In the presence of noise, on the other hand, the unwrapped vector will not generally lie in $K + L$ (but for low-to-moderate noise will be in the vicinity). Thus we search for vector(s) β^* which are as close to $K + L$ as possible in a weighted least-squares sense (Lannes & Anterrieu 1999), i.e. we search for the vector

$$\tau_{RSC} = \begin{bmatrix} \hat{\theta}_{RSC} \\ \hat{\phi}_{RSC} \end{bmatrix} = argmin_{e,\theta,\phi} \left\| \mathbf{W} \left(\beta^*(e) - \mathbf{M} \begin{bmatrix} \theta \\ \phi \end{bmatrix} \right) \right\|^2 \tag{4}$$

where $\mathbf{W}$ is the weighting matrix. If we let Σ denote the phase measurement covariance matrix and set $\mathbf{W} = \Sigma^{-1}$, this is equivalent to searching for vectors $\boldsymbol{e}$ which minimize the projection of a whitened measurement $\mathbf{W}^{\frac{1}{2}}\beta^* = \mathbf{W}^{\frac{1}{2}}(\beta + 2\pi \boldsymbol{e})$ onto the space $(K + L)^{\perp}_{\mathbf{W}} := ker((\mathbf{W}^{\frac{1}{2}}\mathbf{M})^T)$, where $ker(\mathbf{A})$ denotes the kernel, or nullspace, of the matix $\mathbf{A}$. Specifically we seek to minimize:

$$f(\boldsymbol{e}) = ||\mathbf{P}_{\mathbf{W}} \mathbf{W}^{\frac{1}{2}} (\beta + 2\pi \boldsymbol{e})||^2 \tag{5}$$

where $\mathbf{P}_{\mathbf{W}}$ is a matrix representing the orthogonal projection from $\mathbb{R}^n$ onto $(K + L)^{\perp}_{\mathbf{W}}$.

Letting $\boldsymbol{e}' = -\boldsymbol{e}$, we can rewrite the above objective function as:

$$f(\boldsymbol{e}') = ||\mathbf{P_W}\mathbf{W}^{\frac{1}{2}}(\beta - 2\pi\boldsymbol{e}')||^2 = ||\mathbf{P_W}\mathbf{W}^{\frac{1}{2}}\beta - 2\pi\mathbf{P_W}\mathbf{W}^{\frac{1}{2}}\boldsymbol{e}'||^2 \tag{6}$$

Lannes & Anterrieu (1999) showed that this optimization problem is equivalent to the so-called *closest vector problem* in the theory of lattices. We will define a lattice $\mathbf{L}(\mathbb{Z}^n)$ as the set of points generated by integer combinations of the column vectors of a matrix $\mathbf{L}$. Letting $\tilde{\mathbf{P}} = \mathbf{P}_W\mathbf{W}^{\frac{1}{2}}$, our optimization problem then amounts to the following: Find the lattice point in $\tilde{\mathbf{P}}(\mathbb{Z}^n)$ which is closest to $\tilde{\mathbf{P}}\beta$. A compact representation of the lattice Γ is given by:

$$\Gamma = \left\{ \sum_{i=1}^{m \le n-(d+N-3)} a_i \boldsymbol{v}_i \mid \forall a_i \in \mathbb{Z} \right\} \tag{7}$$

where $\{\boldsymbol{v}_i\}$ are linearly-independent and together form a *basis* of the lattice. Given the lattice basis, several algorithms exist for finding the closest lattice point to a specified vector. A popular class of algorithms, known as the Sphere-Decoding algorithms, are efficient searches for the closest lattice point within a hypersphere of a certain radius centered on the input vector (see e.g. Agrell et al. (2002)). For the simulations in this paper, we instead use the lower-complexity Babai Nearest Plane (Babai-NP) algorithm (Babai 1986). For lattice bases which are nearly orthogonal (such as those we use for our simulations), this algorithm offers reliable, albeit not guaranteed, performance in practice.

Suppose we have found a basis for the lattice $\tilde{\mathbf{P}}(\mathbb{Z}^n)$, and we have solved the Closest Vector Problem for a given measurement vector β. Let $\boldsymbol{b}^*$ be the output of the Babai Nearest Plane Algorithm - i.e. it is the lattice point which is the closest to β. We now seek to solve for the wrap vector corresponding to this lattice point, i.e. we seek a solution to:

$$\boldsymbol{b}^* = \tilde{\mathbf{P}}\hat{\boldsymbol{e}} \tag{8}$$

Note that $\tilde{\mathbf{P}}$ is a (weighted) projection matrix and thus not full-rank, and therefore there will be infinitely-many solutions to this equation. The Closest-Vector-Problem algorithm will provide one particular solution $\boldsymbol{e}_p$. The complete set of solutions is then given by:

$$\hat{\boldsymbol{e}} = \boldsymbol{e}_p + \boldsymbol{e}_h \tag{9}$$

where $\boldsymbol{e}_h$ is any integer vector in the kernel of $\tilde{\mathbf{P}}$. Suppose we choose one such vector $\boldsymbol{e}_h$ and correct our phase measurement vector accordingly. The corrected phase measurement vector can be written as:

$$\hat{\beta}^* = \beta + 2\pi(\boldsymbol{e}_p + \boldsymbol{e}_h) \tag{10}$$

Lemma 2.1: $\boldsymbol{e}_h \in K + L, \forall \boldsymbol{e}_h$

Proof: The fact that $\boldsymbol{e}_h \in ker(\mathbf{P_W}\mathbf{W}^{\frac{1}{2}})$ implies that $\mathbf{W}^{\frac{1}{2}}\boldsymbol{e}_h \in ker(\mathbf{P_W})$. This in turn implies that $\mathbf{W}^{\frac{1}{2}}\boldsymbol{e}_h \in im(\mathbf{W}^{\frac{1}{2}}\mathbf{M})$ and hence that $\boldsymbol{e}_h \in im(\mathbf{M})$ since $\mathbf{W}^{\frac{1}{2}}$ is invertible by construction. □

While any choice of $\boldsymbol{e}_h \in K + L$ will admit a solution to Equation (4), let us consider the optimal one $\boldsymbol{e}_{h,0}$ which minimizes the error in the ultimate phase solution τ_{RSC}. Let $\beta_0^* = \beta + 2\pi(\boldsymbol{e}_p + \boldsymbol{e}_{h,0})$ be the corresponding, optimal unwrapped measurement vector. From Lemma 2.1, we see that the unwrapped vector $\hat{\beta}^*$ differs by some $2\pi\boldsymbol{e}_h$ in $K + L$ from β_0^*, i.e.

$$\hat{\beta}^* = \beta_0^* + 2\pi\boldsymbol{e}_h \tag{11}$$

The impact of this fundamental ambiguity is the main subject of this paper. We have depicted the situation in Figure 5 to provide a visual summary of the linear algebra involved. As we have seen, the RSC process begins with the interferometric phase measurement β, which due to wrapping will in general lie far from the range $K + L$ of the measurement matrix. By solving the Closest-Vector-Problem using a lattice algorithm such as the Babai Nearest Plane algorithm, it is possible to find a particular correction vector $2\pi\boldsymbol{e}_p$ which when added to β minimizes the residual in Equation (4), i.e. the weighted distance from $K + L$. In the noiseless case, this unwrapped vector $\hat{\beta}^*$ will lie in $K+L$ (i.e. zero residual), whereas in the noisy case, it will in general remain outside of $K + L$.[3]. In either case, the choice of the residual-minimizing vector $\hat{\beta}^*$ is not unique. To see this, let the smallest possible residual norm among all unwrapped candidates be denoted as r_{min}. The set of unwrapped measurement vectors r_{min} away from $K + L$ can be represented as discrete points in a plane parallel to $K + L$, each of which corresponds to a distinct choice of $\boldsymbol{e}_p$. Within this family, consider the optimum vector β_0^* whose corresponding least-squares solution τ_{RSC} is minimal. All candidate unwrapped vectors are within an error vector $2\pi\boldsymbol{e}_h^*$ of β_0^*, where $\boldsymbol{e}_h^*$ is an integer vector in $K + L$. RSC algorithms are fundamentally blind to such errors; distinct unwrappings $\hat{\beta}^*$ and β_0^* both produce solutions to Equation (4) in the noiseless case, as do their respective projections onto $K + L$, $\hat{\beta}_{K+L}^*$ and $\hat{\beta}_{0,K+L}^*$, in the noisy case. The property of wrap-invariance introduced in this paper ensures that the effect of such an error on the phase of the resulting RSC solution τ_{RSC} is either: merely a benign integer multiple of 2π (c.f. Section 2.2), or a linear gradient in the estimated Fourier phases, which is equivalent up to an extra image shift (c.f. Section 4) in the reconstructed image. In order to develop conditions for wrap-invariance as they relate to pattern design, we must first characterize the effect of the residual wrap error on the RSC least-squares solution. This is the aim of the next section.

2.2 Quantifying the Effect of the Fundamental Ambiguity

Let us now quantify the effect of this unresolved wrap error on the ultimate least-squares solution, which can be accomplished in two easy steps. Following standard least-squares principles, we first find

[3] Without loss of generality, we have selected $\boldsymbol{e}_h = 0$ in Equation (9) so as to simplify the diagram

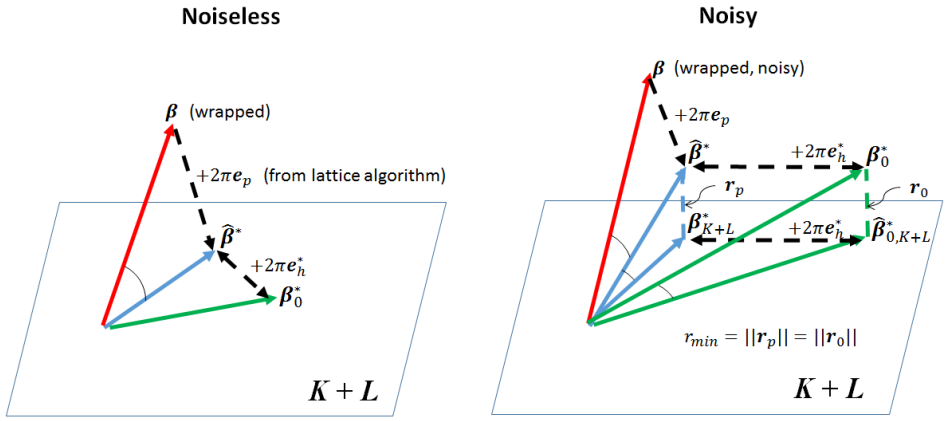

Figure 5. Illustration of the fundamental ambiguity of 2π-periodicity in RSC imaging. Distinct unwrappings $\hat{\beta}^*$ and β_0^* both produce solutions to Equation (4) in the noiseless case, as do their respective projections onto $K+L$, $\hat{\beta}^*_{K+L}$ and $\hat{\beta}^*_{0,K+L}$, in the noisy case.

the projection $\hat{\beta}^*_{K+L}$ of the unwrapped $\hat{\beta}^*$ onto $K+L$ whose weighted distance from $\hat{\beta}^*$ is minimized. Note that the e_h^* term in $\hat{\beta}^*$ is already in $K+L$ and hence unchanged by projection. Hence we obtain:

$$\hat{\beta}^*_{K+L} = \mathbf{W}^{-\frac{1}{2}}(\mathbf{I} - \mathbf{P}_W)\mathbf{W}^{\frac{1}{2}}\hat{\beta}^* = \beta^*_{0,K+L} + 2\pi e_h^* \tag{12}$$

where $\beta^*_{0,K+L}$ is the projection of $\hat{\beta}^*$ onto $K+L$. We then solve the system:

$$\mathbf{M}\begin{bmatrix}\theta\\ \phi\end{bmatrix} = \hat{\beta}^*_{K+L} \tag{13}$$

As aforementioned, $\mathbf{M}$ is rank-deficient (by 3), and hence there will be infinitely-many solutions to this system. Successful recovery of the Fourier phases modulo 2π requires a solution preserving the integrality of the error term e_h^*. In this case, we obtain a final RSC solution $2\pi c$ away from the true solution for some integer vector $\boldsymbol{c}$. To achieve this, we rely on the integer matrix decomposition known as the *Smith Normal Form*, which is described in the following Theorem and Lemma:

Theorem 2.2 (Smith Normal Form) (Smith 1861): Let $\mathbf{A}$ be a nonzero $m \times n$ integer matrix with rank r. There exist integer and unimodular [4] (and thus invertible) matrices $m \times m$ and $n \times n$ matrices $\mathbf{U}$ and $\mathbf{V}$ respectively such that the matrix product $\mathbf{D} = \mathbf{UAV}$ is a diagonal matrix whose diagonal entries $\mathbf{D}_{ii}$ (the so-called *elementary divisors*) are **non-zero integers** for $i \leq r$, and zero for $i > r$.

Lemma 2.3 (Elementary Divisors) (Smith 1861): The product of the elementary divisors is the greatest common divisor (gcd) of all $r \times r$ minors of $\mathbf{A}$.

The proof of the Theorem and Lemma above can be found in textbooks such as Newman (1972). □

Let us compute the Smith Normal Form (SNF) $\{\mathbf{U}, \mathbf{D}, \mathbf{V}\}$ of our matrix $\mathbf{M}$. **Let $\mathbf{U}_M = \mathbf{U}^{-1}$ and $\mathbf{V}_M = \mathbf{V}^{-1}$ so that we can write:**

$$\mathbf{M} = \mathbf{U}_M \mathbf{D}_M \mathbf{V}_M \tag{14}$$

where the r diagonal elements $\{d_i\}$ of $\mathbf{D}_M$ are the elementary divisors of $\mathbf{M}$.

We can now re-write Equation (13) above as:

$$\mathbf{D}_M \mathbf{V}_M \begin{bmatrix}\theta\\ \phi\end{bmatrix} = \mathbf{U}_M^{-1}\hat{\beta}^*_{K+L} \tag{15}$$

Let us choose the following particular solution to Equation (15):

$$\tau_{RSC} = \mathbf{V}_M^{-1}\mathbf{D}_M^{+}\mathbf{U}_M^{-1}\hat{\beta}^*_{K+L} \tag{16}$$

where $\mathbf{D}_M^+$ denotes the pseudo-inverse of $\mathbf{D}$. The resulting error is then:

$$e_{RSC} = \mathbf{V}_M^{-1}\mathbf{D}_M^{+}\mathbf{U}_M^{-1}e_h^* \tag{17}$$

Lemma 2.4: Let $\boldsymbol{u} = \mathbf{U}_M^{-1}e_h^*$. The residual wrap error $\boldsymbol{e}_{RSC}$ equals $\vec{0} \mod 2\pi$ if and only if $\mod(u_i, d_i) = 0, \forall i \leq r$. The proof of this Lemma is an adaptation of a standard proof which can be found in most textbooks covering linear Diophantine equations (see, e.g. Newman (1972)). □

From this Lemma, the following Corollary is clear:

Corollary 2.5 ***(Sufficient condition on SNF of RSC matrix for wrap-invariance)***: If the elementary divisors of the measurement matrix $\mathbf{M}$ corresponding to a certain aperture pattern are all 1, the RSC solution defined by τ_{RSC} is immune to phase-wrapping error.

□

RSC patterns consisting of apertures placed randomly on a Cartesian grid appear to satisfy this sufficient condition with high probability. We conducted a simple experiment in which 15 apertures were randomly placed on a 10×10 grid. Out of 256 placements, 66 were valid RSC patterns (i.e. possessed at least critical redundancy), and of these, only 2 had non-unity elementary divisors.

[4] A unimodular matrix is one whose determinant is ±1

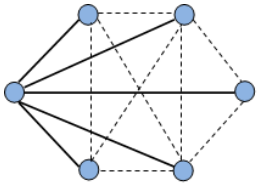

Figure 6. Distinction between spanning tree baselines (thick, solid) and loop entry baselines (thin, dotted)

2.3 Relation to closure-phase approaches

The SNF has been been applied to the RSC phase problem before (Lannes 2003). Whereas we have chosen to apply SNF directly to the baseline measurement matrix, the approach taken by Lannes (2003) is to instead treat the piston-invariant phases of the bispectra (the so-called *closure phases*) as the fundamental observables from which the object phases can be inferred via the relation:

$$\mathbf{C}_{o\to c}\vec{\theta} = \boldsymbol{y}_{cl} + 2\pi \boldsymbol{e}_{cl} \tag{18}$$

where $\boldsymbol{y}_{cl}$ are the wrapped closure phases, $\boldsymbol{e}_{cl}$ is the corresponding wrap vector, and $\mathbf{C}_{o\to c}$ is the matrix mapping the distinct object phases in the array to closure phases. Lannes (2003) hence applies the SNF to the closure matrix $\mathbf{C}_{o\to c}$. By direct analogy to Corollary 2.5, note that if the elementary divisors of $\mathbf{C}_{oc}$ are all 1, then the RSC solution is immune to phase-wrapping error. Using closure phases as observables can be advantageous in low-light scenarios in which there is not sufficient SNR in a single atmospheric coherence time to reliably measure the baseline phases. To overcome this low per-frame SNR, atmosphere-invariant observables such as the bispectra can be integrated over many frames to build sufficient SNR, and their respective closure phases used as reliable phase measurements. Since the baseline phases are known modulo 2π, the linear combinations of them which comprise the closure phases are also known modulo 2π. In order to relate this condition to Corollary 2.5, let us first define another closure matrix $\mathbf{C}_{m\to c}$ which instead maps the phase measurements to closure phases. This mapping consists of equations of the form:

$$y_{123} = \beta_{12} + \beta_{23} - \beta_{13} \tag{19}$$

where y_{123} is the closure phase associated with apertures 1, 2, and 3, and the β_{ij} are the associated baseline phases (see Equation (1)). Of the $\binom{n}{3}$ possible closure phases, at most $\binom{n-1}{2}$ can be linearly-independent (see e.g. Readhead et al. (1988)). One commonly-chosen set of such linearly-independent relations consists of all the closure triangles involving a given aperture A, and this is the set selected by Lannes (2003). $\mathbf{C}_{m\to c}$ is therefore an $\binom{n-1}{2}\times\binom{n}{2}$ matrix. Lannes (2003) accordingly provides a convenient grouping of the baselines into two categories: (1) *spanning tree* baselines which connect aperture A to all other apertures, and (2) *loop entry* baselines which provide the closure for these spanning tree baselines. This categorization is depicted in Figure 6.

Given this categorization, we can decompose $\mathbf{C}_{m\to c}$ into corresponding blocks as:

$$\mathbf{C}_{m\to c} = \begin{bmatrix} \hat{\mathbf{C}}_{m\to c} & \mathbf{I}_{\binom{n-1}{2}} \end{bmatrix} \tag{20}$$

where $\hat{\mathbf{C}}_{m\to c}$ contains the spanning tree contributions to the matrix (which appear in multiple closures), and $\mathbf{I}_{\binom{n-1}{2}}$ is the $\binom{n-1}{2}\times\binom{n-1}{2}$ identity matrix representing the loop-entry contributions (each of which appears in only one closure). The following property follows from this block form expression:

Lemma 2.6: The elementary divisors of $\mathbf{C}_{m\to c}$ are all 1.

Proof: Since we have chosen a linearly-independent subset of closure relations, $r = rank(\mathbf{C}_{m\to c}) = \binom{n-1}{2}$. There exists a $r\times r$ minor (namely, $\mathbf{I}_{\binom{n-1}{2}}$) which is equal to 1. Therefore the gcd of all $r\times r$ minors is 1, and therefore from Lemma 2.3 (Elementary Divisors), all elementary divisors must be 1. □

Let us now relate $\mathbf{C}_{m\to c}$ to the matrix $\mathbf{C}_{o\to c}$ used by Lannes (2003). Recall from the discussion of bispectra in Section 1 that the closure relations eliminate piston differences in the measurements so that $\mathbf{C}_{m\to c}$ annihilates the subspace L, i.e. the space spanned by the columns of $\mathbf{M}$ corresponding to $\vec{\phi}$. Defining $\mathbf{M}_\theta$ as the submatrix of $\mathbf{M}$ containing the columns corresponding to $\vec{\theta}$, we have

$$\mathbf{C}_{m\to c}\mathbf{M}\begin{bmatrix}\theta\\ \phi\end{bmatrix} = \begin{bmatrix}\mathbf{C}_{o\to c} & \boldsymbol{0}\end{bmatrix}\begin{bmatrix}\theta\\ \phi\end{bmatrix} \tag{21}$$

where $\mathbf{C}_{o\to c} = \mathbf{C}_{m\to c}\mathbf{M}_\theta$. $\mathbf{C}_{o\to c}$ is an $\binom{n-1}{2}\times d$ matrix which is rank-deficient by two [5].

Then by direct analogy to Equation (13), we can obtain valid RSC object phase solutions by solving:

$$\mathbf{C}_{m\to c}\mathbf{M}\begin{bmatrix}\theta\\ \phi\end{bmatrix} = \begin{bmatrix}\mathbf{C}_{o\to c} & \boldsymbol{0}\end{bmatrix}\begin{bmatrix}\theta\\ \phi\end{bmatrix} = \boldsymbol{y}^*_{cl} + 2\pi \boldsymbol{e}^*_{h,cl} \tag{22}$$

where $\boldsymbol{y}^*_{cl}$ is the true unwrapped closure vector and $2\pi\boldsymbol{e}^*_{h,cl}$ is the residual integer wrapping error vector after applying the Babai NP algorithm to solve the CVP problem associated with matrix $\mathbf{C}_{m\to c}\mathbf{M}_\theta$ and $2\pi\boldsymbol{e}_{cl}$. Note that if we find a vector $\vec{\theta}^*$ satisfying Equation (22), it will clearly also satisfy the relation $\mathbf{C}_{o\to c}\vec{\theta}^* = \boldsymbol{y}^*_{cl} + 2\pi\boldsymbol{e}^*_{h,cl}$ of Lannes (2003). Note furthermore that we can solve the equation above in two separate integer-preserving steps of the form of Equation (16), the first involving the SNF decomposition of $\mathbf{C}_{m\to c}$, and the second involving that of $\mathbf{M}$. Since the elementary divisors of $\mathbf{C}_{m\to c}$ are all 1 by construction (by Lemma 2.6) and hence the first step is thus integer-preserving, wrap-invariance again amounts to whether or not all elementary divisors of $\mathbf{M}$ are 1. Therefore we have the following Proposition relating wrap invariance for closure measurements to that for raw phase measurements:

Proposition 2.7 ***(Sufficient condition for wrap-invariance of closure-based RSC)***: If the elementary divisors of the phase measurement matrix $\mathbf{M}$ are all 1, then the closure-based RSC solution will be wrap-invariant. □

We remark in passing that although the preceding analysis was presented in the context of the traditional three-aperture closure, it applies directly to the case of closures involving an arbitrary number of sides. As an example, consider the pattern shown in Figure 7. A spanning tree for the pattern consisting of the short baselines in an array is

[5] To see this, note that each solution set to Equation (18) above remains valid after replacing each θ_{ij} with $\theta^p_{ij} = \theta_{ij} - \boldsymbol{z}\cdot(\boldsymbol{r}_j - \boldsymbol{r}_i)$

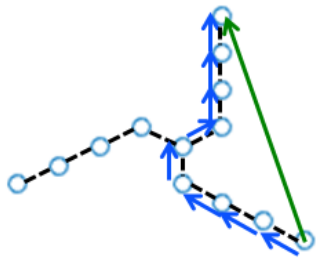

Figure 7. Bootstrapping phase of a low-SNR baseline (green) with subset (blue) of high-SNR baselines from spanning tree baselines (black)

depicted. Let $\{\phi_{sp}\}$ denote the aperture phase differences in these $n-1$ spanning tree baselines. Note that all aperture phase differences in the array can be expressed as linear combinations of the $\{\phi_{sp}\}$. If the aperture phase differences are known reliably via measurements of the spanning tree baselines, we can use these measurements to cancel the aperture phase differences in all other measurements (of which one example is shown in green). The idea of using such *generalized closure phases* (Martinache 2010) is indeed the mathematical foundation for the promising technique known as *baseline bootstrapping* in which high-fidelity phase measurements of several high-SNR baselines (typically the short baselines) to cancel the atmosphere on each lower-SNR (and hence lower fidelity) baseline.

Note that for an arbitrary n-aperture pattern, there will in general be $n-1$ spanning tree baselines and thus $\binom{n}{2} - (n-1) = \binom{n-1}{2}$ generalized closures, each involving a distinct closing (or loop-entry) baseline. Therefore the resulting measurement matrix can be expressed exactly as in Equation (20) above and hence the preceding analysis holds.

While this section has considered a few possibilities for phase observables, relating mathematical conditions for wrap invariance to a physical condition on aperture placement is more intuitive when considering the raw phase measurements as opposed to their closures. For this reason, for the remainder of the paper we will work directly with the baseline phases and their associated wrapping errors. In particular, we will begin by connecting these wrapping errors with analogous ambiguities in recently-developed phasor-based approaches.

3 IMPLICATIONS OF WRAP AMBIGUITIES ON PATTERN DESIGN

In this section we use the mathematically-sufficient conditions for wrap invariance from the previous section to show that aperture patterns whose interferometric graph satisfies a certain loop-free condition are wrap-invariant. Here we define the *interferometric graph* in the standard way: it is simply the graph formed by connecting the array's apertures (the *nodes* of the graph) with edges representing the array's baselines.

This condition is founded on the **Lemma 2.3 (Elementary Divisors) in Section 2** and the following definition of the matrix determinant. This definition is given in many linear algebra texts (see e.g. Bretscher (2001)).

Definition 3.1 : Suppose we have an $n \times n$ matrix $\mathbf{A}$. Define a *pattern* as a selection of n entries of the matrix in which there is only one chosen entry in each row and one in each column of the matrix. Furthermore, we denote a pair of numbers in a pattern as *inverted* if one of them is located above and to the right of the other. Then we can obtain the determinant of $\mathbf{A}$ by summing the products associated with all patterns with an even number of inversions and subtracting the products associated with all the patterns with an odd number of inversions.

Consider a $r \times r$ sub-matrix $\tilde{\mathbf{M}}_I$ consisting of a set I of linearly-independent rows in $\mathbf{M}$ and $d+N-3$ linearly-independent columns. Our goal will be to find conditions under which such a sub-matrix contains only one pattern with a non-zero product, in which case the determinant will be ± 1 from the definition above. **This will guarantee, by the Lemma 2.3 (Elementary Divisors) of the previous section, that the elementary divisors of $\mathbf{M}$ are all 1, which will in turn ensure that the error in the RSC solution τ_{RSC} will be $0 \mod 2\pi$ by Corollary 2.5.**

Consider one such $\tilde{\mathbf{M}}_I$ and note that within the fully-connected interferometric graph associated with $\mathbf{M}$, we can identify a sub-graph G containing only the measurements in $\tilde{\mathbf{M}}_I$. This will be done by sequentially identifying those matrix entries which must be part of a pattern with a non-zero product. Note that some of these special entries from the matrix $\tilde{\mathbf{M}}_I$ can be identified immediately. Namely, all non-redundant measurements contain a singleton ± 1 in the column associated with their object phase. All non-zero patterns must clearly contain this ± 1 and so we can select these singleton object-phase entries as guaranteed participants in a non-zero pattern. Moreover, all measurements containing a *leaf node* (i.e. a node with a single connection) in G contain a singleton ± 1 in the column associated with their leaf node. All non-zero patterns must clearly contain this ± 1 as well. Thus we can also select these leaf node entries as guaranteed participants in a non-zero pattern.

There may be cascading implications of such singleton measurements. To illustrate this, consider the scenario shown in Figure 8. A simple RSC array is shown on the left. A subset of the baselines in one possible linearly-independent sub-matrix $\mathbf{M}_I$ is depicted. Here we intentionally defer selection of the arbitrarily-set phases until later for purposes of generality. A simplified depiction of the matrix $\mathbf{M}_I$ is shown in which all non-zero entries have been colored black and all zero entries have been colored white for simplicity. In Step A of the reduction process, object phase θ_5 is selected for participation (i.e. its matrix entry factored as common to all non-zero patterns) since it is a singleton object phase. Its corresponding row (i.e. row 5) in $\mathbf{M}_I$ is then eliminated from participation since the remaining entries in this row cannot participate in a pattern (by definition of a pattern). In Step B, the aperture 6 entry ϕ_6 in row 5 is selected since it has become a leaf node in the pattern, and row 5 can then be eliminated. Then in Step C, object phase θ_4 is then selected by virtue of becoming a singleton object phase, and row 4 is then eliminated. This selection/elimination process can be repeated beyond the steps shown in the Figure, until either no leaf nodes and singleton object phases remain, or there are no baselines left

to eliminate. We formalize the *pattern reduction* process in Algorithm 1 below.

Algorithm 1 Pattern Reduction Algorithm

Require: R {where R is the set of the baselines corresponding to $\mathbf{M}_I$, where I denotes the indices of a linearly-independent subset of $d+N-3$ rows of $\mathbf{M}$}
  while $|R| > 0$ **do**
    1. **Leaf Nodes**
    1.1 remove any remaining baselines containing leaf nodes from R
    1.2 add the associated apertures to the list N
    2. **Singleton Object Phases**
    2.1 remove any remaining baselines containing singleton object phases from R
    2.2 add the associated object phases to the list O
    if no baselines removed in the current iteration **then**
      return PERSISTENT
    end if
  end while
  return LOOPFREE

We can see that any baseline in an interferometric graph which does not belong to a loop will be eliminated in the reduction process, and its corresponding matrix entries factored. The only structures in the graph that persist after this reduction are sets of loops with a certain property. Namely we define a *persistent loop set* as a set of loops that contains at least two instances of every baseline contained in the set. (A set can consist of any number of loops, including one). With this definition, absolute invariance may be possible if the graph of the redundant baselines does not contain any persistent loop sets. Algorithm 1 returns PERSISTENT if persistent loops exist and LOOPFREE if the pattern is completely reduced and therefore free of persistent loops.

Note that in the latter case, we will have eliminated r rows from $\mathbf{M}_I$. Since each baseline elimination is associated with object phase or aperture selection from distinct columns, and $\mathbf{M}_I$ contains $r+3$ columns, there will be exactly three extraneous columns not involved in the reduction process. The $r \times r$ submatrix obtained by selecting the non-extraneous columns (i.e. those corresponding to the selected object phases and leaf nodes in O and N, respectively) will then **have a determinant of** ± 1 by virtue of having a single non-zero pattern revealed by the reduction process. Having ensured the existence of a unit $r \times r$ minor, **the gcd of all $r \times r$ minors must be 1. We have hence confirmed the elementary divisors must be all 1, and thereby ensured that the pattern is wrap-invariant (c.f. Lemma 2.3 (Elementary Divisors), and Corollary 2.5).** We summarize the sufficient condition as follows:

Proposition 3.2 ***(Sufficient conditions on aperture pattern for wrap-invariance)***: Consider the graph of an aperture pattern which contains d distinct baselines and any set of $N-3$ linearly-independent redundant baselines. If this graph does not contain persistent loop sets (in the sense defined above), the matrix $\tilde{\mathbf{M}}_I$ formed by these independent measurements will have determinant ± 1. As a result **Corollary 2.5 will hold, thereby guaranteeing that RSC solution τ_{RSC} will be invariant to wrapping of the phase measurements.**

We have hence arrived at a a physical definition of a *wrap-invariant* pattern. We now apply Algorithm 1 to the example pattern shown in Figure 2. Algorithm 1 reduces the pattern to the persistent loop set shown in Figure 9.

The elementary divisors of the pattern's measurement matrix are not all 1; they are all 1 except for a singleton 3 and hence $det(\tilde{\mathbf{M}}_I) \mod 3 = 0$ for all choices of $\tilde{\mathbf{M}}_I$.

Having traced the distortion induced by phase wrapping to physical property of the array itself, we now return to Figure 3. The lower left panel shows the reconstruction result with the SNF-based Phase method described in Section 2. The closure phase approach yields the same corruption in reconstruction, as the elementary divisors of $\mathbf{C}_{oc}$ are also all 1 except for a singleton 3.

There are several simple ways to amend this pattern so that it is wrap-invariant. While the most intuitive of these involve moving the apertures involved in the persistent loop shown in Figure 9, these approaches leave gaps in the UV-sampling pattern. An alternate approach that preserves the UV-sampling is to add an aperture to the center of the pattern as shown in Figure 10. This results in additional linearly-independent redundancies colored in blue and green, respectively, in the Figure. These additions replace baselines in the persistent loop, allowing this loop to be broken. With wrap-invariance, reconstruction results match the true image in both the phase and phasor approaches as respectively shown in Figure 11. In the top row, reconstruction results are displayed for the phase (left) and phasor (right) approaches for the noiseless case. **The image distortion present in Figure 3 has been completely eliminated by tweaking the pattern so that it is wrap-invariant.** Analogous results for an SNR of 25 dB are displayed in the bottom row. Here we define SNR as the ratio of the phasor magnitude at visibility 1 (i.e. zero spatial frequency) to the standard deviation of the noise, which we have assumed to be complex Gaussian and i.i.d. across spatial frequency for this simulation.

4 WRAP-INVARIANCE AND PRACTICAL RSC CALIBRATION

In previous sections we established that the Phase Approach can be made robust to phase-wrapping using the Smith Normal Form (SNF) and algorithms from lattice theory. Moreover, the SNF provided a mathematical framework for the notion of wrap-invariance. From a practical standpoint, however, computation of the Smith Normal Form is likely to become a computational burden for large arrays, as in those under current consideration with $N_{ap} \approx 10^2$ and $n \approx 10^4$ baselines (Zheng et al. 2014). Techniques not requiring such a computation are hence of strong practical interest. In this section we show that the wrap-invariance property checked by Algorithm 1 provides a certificate for reliable reconstruction with such techniques, in the presence of the fundamental 2π-periodicity of interferometric measurements.

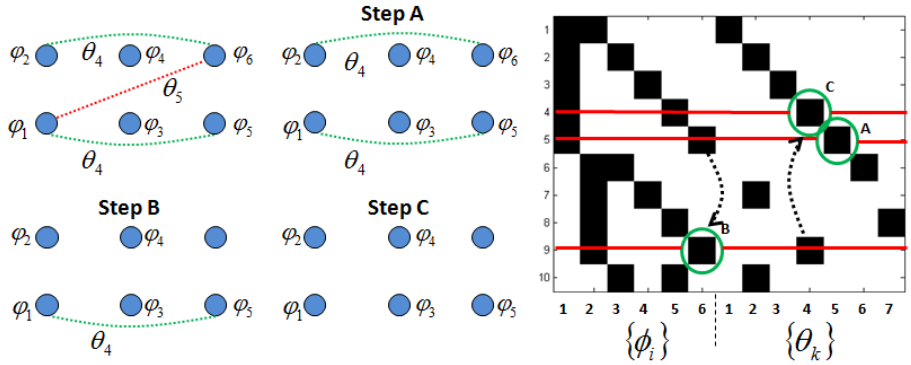

Figure 8. Example: Reducing an aperture pattern and associated matrix to identify Persistent Loop(s)

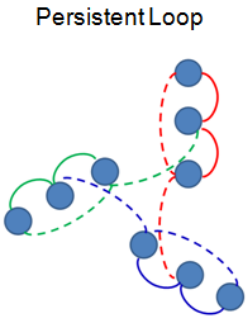

Figure 9. Persistent Loop set at center of pattern in Figure 2

Figure 10. Amended Pattern

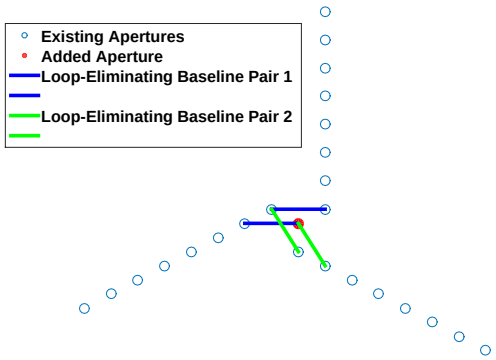

4.1 Practical Phase Approaches

Our approach here will rely upon the well-known Singular Value Decomposition (SVD) of the measurement matrix $\mathbf{M}$, which is given by:

$$\mathbf{M} = \mathbf{U}_\sigma \Sigma_\sigma \mathbf{V}_\sigma \tag{23}$$

in which $\mathbf{U}_\sigma$ and $\mathbf{V}_\sigma$ are $m \times m$ and $(d+N) \times (d+N)$ orthogonal matrices, respectively. Σ_σ is a $m \times (d+N)$ diagonal matrix with r non-zero diagonal entries (the so-called *singular values of* $\mathbf{M}$), where $r = rank(M) = d + N - 3$.

Lemma 4.1: The final 3 columns of $\mathbf{V}_\sigma$ form a basis for the nullspace of $\mathbf{M}$.

Proof: This follows from the fact $\mathbf{M}$ is rank-deficient by 3, and standard properties of the right singular vectors comprising $\mathbf{V}_\sigma$ in the SVD. (Bretscher 2001) □

Now recall that in Section 2, we provided an one particular, SNF-based, solution to Equation (13). Here we instead consider the complete set of solutions to this Equation, which is given by:

$$\tau_\sigma = \mathbf{M}^+ (\hat{\beta}^*_{0,K+L} + 2\pi e^*_h) + \tau_0 \tag{24}$$

where τ_0 is any vector in the nullspace of $\mathbf{M}$, and $\mathbf{M}^+$ denotes the pseudo-inverse of $\mathbf{M}$, whose matrix elements are derived directly from the SVD above.

$$\mathbf{M}^+ = \mathbf{V}_\sigma \Sigma^+_\sigma \mathbf{U}^T_\sigma \tag{25}$$

where Σ^+_σ is a $(d+N) \times m$ diagonal matrix whose r non-zero diagonal entries are the reciprocals of the corresponding non-zero entries in Σ^+_σ.

Typically Phase Approach techniques implicitly select a particular solution from the family of solutions in Equation (24) via augmenting the matrix $\mathbf{M}$ with additional constraints. The most common among these (Wieringa 1992) (Wijnholds & Noorishad 2012) is to enforce that: $\sum \phi = 0$, $\sum \phi_i \boldsymbol{r}_i = \boldsymbol{0}$, where $\boldsymbol{r}_i$ is the vector position of the i-th aperture in the array.

Note that the error resulting from application of this

Figure 11. Reconstruction Results for Amended Pattern

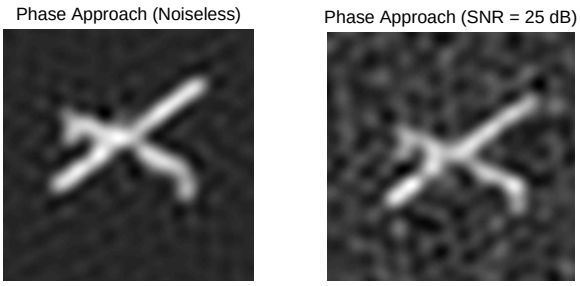

pseudo-inverse to the unwrapped measurement vector will be given by:

$$2\pi \boldsymbol{e}_{\sigma} = \mathbf{M}^{+}(2\pi \boldsymbol{e}_{h}^{*}) \tag{26}$$

Recall that the error vector $\boldsymbol{e}_{\sigma}$ has two parts: one for the error in the atmosphere/piston (which we will denote with the index L), and one for the error in the Fourier phases (which we denote with the index K), i.e.:

$$\boldsymbol{e}_{\sigma} = [\boldsymbol{e}_{\sigma,L}, \boldsymbol{e}_{\sigma,K}]^{T} \tag{27}$$

We will focus attention on the latter, since it is of direct relevance for image formation. Let us express the spatial frequencies measured by an array as two-element vectors of the form (ω_x, ω_y). Let $\mathbf{X}$ be the $d\times 2$ matrix containing these spatial frequencies. Note then that the phase-wrap error will manifest itself merely as an image shift if and only if this error is a (modulo-2π) phase ramp, i.e. there exists a 2-element shift vector $\boldsymbol{z}$ and an integer vector $\boldsymbol{k}$ which together satisfy:

$$2\pi \boldsymbol{e}_{\sigma,K} - 2\pi \mathbf{X}\boldsymbol{z} = 2\pi \boldsymbol{k} \tag{28}$$

Substituting from Equation (26) we obtain:

$$\mathbf{M}_{K}^{+}(2\pi \boldsymbol{e}) - 2\pi \mathbf{X}\boldsymbol{z} = 2\pi \boldsymbol{k} \tag{29}$$

where $\mathbf{M}_{K}^{+}$ denotes the sub-matrix of $\mathbf{M}^{+}$ formed by the rows associated with K.

Dividing through by 2π we obtain the equation: $\mathbf{M}_{K}^{+}\boldsymbol{e}_{h}^{*} - \mathbf{X}\boldsymbol{z} = \boldsymbol{k}$. Note that each element of $\mathbf{M}_{K}^{+}$ can be expressed as some rational number $\frac{p_i}{q_i}$. Similarly we first assume $\mathbf{X}$ contains rational spatial frequencies with greatest common denominator q_x. Then we can multiply through by the least-common-multiple (LCM) of the $\{q_i\}$ and q_x to obtain a system of equations whose coefficients are guaranteed to be integer (i.e., we have a linear Diophantine system). Let this LCM be denoted as l. Then we have, after rearranging terms,

$$l\mathbf{X}\boldsymbol{z} = l(\mathbf{M}_{K}^{+}\boldsymbol{e}_{h}^{*} - \boldsymbol{k}) \tag{30}$$

We now wish to determine conditions under which there exist vectors $\boldsymbol{k}$ and $\boldsymbol{z}$ satisfying this overdetermined Diophantine system. Applying the Smith Normal Form decomposition (c.f. Theorem 2.2) to the matrix $l\mathbf{X}$ this time, and noting that $rank(\mathbf{X}) = 2$, we have:

$$\mathbf{D}_{\mathbf{X}} = \mathbf{U}_{\mathbf{X}}(l\mathbf{X})\mathbf{V}_{\mathbf{X}} \tag{31}$$

where $\mathbf{U}_{\mathbf{X}}$ and $\mathbf{V}_{\mathbf{X}}$ are unimodular matrices of size $m\times m$ and 2×2, respectively, and $\mathbf{D}_{\mathbf{X}}$ is a rectangular diagonal matrix whose entries are zero below row 2.

If we left-multiply Equation (30) by $\mathbf{U}_{\mathbf{X}}$ on both sides, we obtain:

$$l\mathbf{U}_{\mathbf{X}}\mathbf{X}\boldsymbol{z} = l\mathbf{U}_{\mathbf{X}}(\mathbf{M}_{K}^{+}\boldsymbol{e}_{h}^{*} - \boldsymbol{k}) \tag{32}$$

Using Equation (31) and the fact that $\mathbf{V}_{\mathbf{X}}$ is a unimodular (and hence invertible) matrix, we can then write:

$$\mathbf{D}_{\mathbf{X}}\mathbf{V}_{\mathbf{X}}^{-1}\boldsymbol{z} = l(\mathbf{U}_{\mathbf{X}}\mathbf{M}_{K}^{+}\boldsymbol{e}_{h}^{*} - \mathbf{U}_{\mathbf{X}}\boldsymbol{k}) \tag{33}$$

We are now in position to prove the main result of this section, which is preceded by the following Lemma:

Lemma 4.2: Given wrap-invariance, the (column) vector $\mathbf{U}_{\mathbf{X}}\mathbf{M}_{K}^{+}\boldsymbol{e}$ has integer entries below row 2.

Proof: (see Appendix) □

Proposition 4.3: If a pattern is wrap-invariant (in the sense of Section 3), reconstruction error induced by phase wrapping is limited to an image shift.

Proof: We re-arrange the Equation (33) above so that it reads:

$$\frac{1}{l}\mathbf{D}_{\mathbf{X}}\mathbf{V}_{\mathbf{X}}^{-1}\boldsymbol{z} - \mathbf{U}_{\mathbf{X}}\mathbf{M}_{K}^{+}\boldsymbol{e}_{h}^{*} = -\mathbf{U}_{\mathbf{X}}\boldsymbol{k} \tag{34}$$

Let $\boldsymbol{v} = \frac{1}{l}\mathbf{D}_{\mathbf{X}}\mathbf{V}_{\mathbf{X}}^{-1}\boldsymbol{z} - \mathbf{U}_{\mathbf{X}}\mathbf{M}_{K}^{+}\boldsymbol{e}_{h}^{*}$. Note that since $\mathbf{D}_{\mathbf{X}}$ is zero below row 2, the entries of $\boldsymbol{v}$ below row 2 will be equal to those of $(-\mathbf{U}_{\mathbf{X}}\mathbf{M}_{K}^{+}\boldsymbol{e}_{h}^{*})$, which are integers by Lemma 4.2. Now consider the first and second entries of $\boldsymbol{v}$. Let $\boldsymbol{f}$ be the vector containing the fractional parts of the first two elements of vector $\mathbf{U}_{\mathbf{X}}\mathbf{M}_{K}^{+}\boldsymbol{e}_{h}^{*}$, and let $\mathbf{A}$ be the invertible matrix consisting of the first two rows of $\frac{1}{l}\mathbf{D}_{\mathbf{X}}\mathbf{V}_{\mathbf{X}}^{-1}$. **Without loss of generality** choose $\boldsymbol{z}^{*} = \mathbf{A}^{-1}\boldsymbol{f}$ so that the fractional part $\boldsymbol{f}$ is annihilated, leaving only integer elements in the first two entries of $\boldsymbol{v}$. Hence we now have:

$$\boldsymbol{v} = -\mathbf{U}_{\mathbf{X}}\boldsymbol{k} \tag{35}$$

with $\boldsymbol{v}$ ensured to contain only integer elements. Since $\mathbf{U}_{\mathbf{X}}$ is unimodular, the vector $\boldsymbol{k}^{*} = -\mathbf{U}_{\mathbf{X}}^{-1}\boldsymbol{v}$ will be integral. We have thus found a pair $(\boldsymbol{z}^{*}, \boldsymbol{k}^{*})$ with integer $\boldsymbol{k}^{*}$ which satisfies the Equation (33). Since Equation (33) is related to Equation (30) via a unimodular (and hence invertible) mapping $\mathbf{U}_{\mathbf{X}}$, invariance is hence proven. □

With the previous result, we have characterized the complete family of Phase Approach solutions given in Equation (24). Namely we have shown that, for a wrap-invariant pattern, the family differs by at most an image shift from the true solution. Returning to our running example in Figure 10, we verified that different solution choices from the family given in Equation (24) simply resulted in shifts of an otherwise pristine image in the reconstruction. On the other hand with wrap-variant pattern in Figure 2, image distortion of the severity of Figure 3 was again observed, as expected.

4.2 Practical Phasor Approaches

Though traditional treatments employ the phase approach of the previous section which operates on baseline phases, recent papers (e.g. Marthi & Chengalur (2014), Liu et al. (2010)) have shown that **approaches which operate at the phasor level can be superior in accuracy**. Liu et al. (2010) developed a Gauss-Newton-type **Non-linear Least-Squares (NLS)** solver and showed it produced unbiased phase estimates, in contrast with the biased ones provided by the phase approach. **Marthi & Chengalur (2014) and Wijnholds & Noorishad (2012) have also proposed low-complexity phasor-based approaches and demonstrated performance near the Cramer-Rao Bound.** Though the capacity of the Phasor approaches to produce superior accuracy relative to Phase approach has been demonstrated, the former's convergence issues can be

mitigated via initialization with the results of the latter (see e.g. Liu et al. (2010), and Zheng et al. (2014)).

The implementations of the Phasor Approach typically employ the following measurement model:

$$V_{ij} = g_i g_j^* f_{ij} + n_{ij} \tag{36}$$

where V_{ij} is the complex visibility observed between apertures i and j, $g_i = |g_i|e^{j\phi_i}$ and $g_j = |g_j|e^{j\phi_j}$ are the complex gains of these apertures, f_{ij} is the true complex visibility measured by this pair, and n is complex measurement noise. Note that the phase difference between g_i and g_j is simply the optical path difference between apertures i and j introduced in the previous section. Given this model, NLS approaches attempt to find a set of complex phasors $\{g_i\}$ and $\{f\}$ which minimize an objective function of the form:

$$\Lambda = \sum_i \sum_{j>i} w_{ij} ||(V_{ij} - g_i g_j^* f_{ij})(V_{ij}^* - g_i^* g_j f_{ij}^*)|| \tag{37}$$

Minimization of Λ with respect to the unknowns (i.e. distinct object and antenna complex gains) **can be accomplished with iterative application of the following updates**, as reported by Marthi & Chengalur (2014) in the context of radio interferometry, and by Lacour et al. (2007) in the context of optical interferometry:

$$g_k = \frac{\sum_{j\neq k} w_{kj} g_j f_{kj}^* V_{kj}}{\sum_{j\neq k} w_{kj} |g_j|^2 |f_{kj}|^2} \tag{38}$$

$$f_b = \frac{\sum_{j>k} g_k^* g_j V_{kj}}{\sum_{j>k} w_{kj} |g_k|^2 |g_j|^2} \tag{39}$$

where the $\{f_b\}$ are the true complex visibilities of the distinct object phases in the array.

Due to the circularity of these definitions, these equations must be solved iteratively. Starting from an initial guess for all phasors, Equation (38) is solved to obtain a better estimate for the $\{g_k\}$ and then these $\{g_k\}$ are used to obtain refined estimates of the $\{f_b\}$ through Equation (39). In the next iteration, these $\{f_b\}$ are used to further refine $\{g_k\}$, and so on.

Though there are other means of minimizing objectives of the form Λ (Wijnholds & Noorishad 2012) (Liu et al. 2010), we omit discussion of them here; our present purpose is to characterize the correctness of the solutions themselves, regardless of how they are obtained. As has been noted before (see e.g. Lannes & Anterrieu (1999)), there are strong connections between phase- and phasor-based approaches. To see this, let $\boldsymbol{z}$ be the vector of products $\{g_i g_j^* f_{|i-j|}\}$ which minimize Λ. We rewrite Equation (37) as:

$$\Lambda = \sum_i \sum_{j>i} w_{ij} ||(V_{ij} - z_{ij})(V_{ij}^* - z_{ij}^*)|| \tag{40}$$

Define $r_{ij} = e^{j2\pi n_{ij}} z_{ij}$ for an arbitrary integer n_{ij} and $\boldsymbol{r}$ as the vector containing the r_{ij}.

Note that $\boldsymbol{r}$ also minimizes Λ since the rotations $\{e^{j2\pi n_{ij}}\}$ do not change the values of the residuals in Λ. Hence any set of rotated phasors $\{\tilde{g}_i\}$ and $\{\tilde{f}_{|i-j|}\}$ whose products produce the vector $\boldsymbol{r}$ will also minimize Λ. Note that the set of such valid phase vectors (i.e. the concatenations of possible $\{\angle\tilde{g}_i\}$ and $\{\angle\tilde{f}_{|i-j|}\}$) includes the complete family of Phase-approach solutions τ_σ in Section 4.1 with $\hat{\beta}_{K+L}^* = \angle\boldsymbol{r}$ (where $\angle\boldsymbol{r}$ is the vector of the phases of the complex vector $\boldsymbol{r}$). **In other words, the valid phase component of the phasor approach solutions is not unique, and the minimization of Λ admits the same solution ambiguity depicted in Figure 5. Hence we see that** integer ambiguities present in the phase approach do not disappear in the phasor approach; in fact, the unwrapped candidate solutions of the phase-based approach correspond to **global minima** of the phasor-based objective. **In practice Phasor Approach techniques may converge to any one of these minima. Hence the critical issue for reliable image reconstruction is again the nature of the difference between these valid minima and the true solutions. Based on the connections we have drawn with Phase-approach solutions above, the following Proposition is clear**:

Proposition 4.4: If a pattern is wrap-invariant, the global minima of the Phasor-Approach objective caused by the inherent 2π-periodicity in the objective's residual differ from the true solution merely by an image shift.

In practice we see that, as in the Phase approach, if the pattern is not wrap-invariant, the Phasor Approach suffers from false global minima producing severe distortion in the resulting reconstruction. The lower right panel of Figure 3 shows the resulting reconstruction produced by the Phasor method using the updates in Equations (38) and (39). To show the correspondence in solutions between two types of approaches, we provided the result of the Phase approach as the initial point for the Phasor approach as is common in practice (Liu et al. 2010), (Zheng et al. 2014). **Indeed this point is a global minimum of Λ which the updates above cannot escape, and as a result we observe virtually-identical distortion to that of the Phase approach.**

We repeated the experiment with the wrap-invariant pattern in Figure 10, and as expected, the results were pristine in the noiseless case and virtually-identical to those of the Phase approach in the noisy case. For completeness the results are given in Figure 12.

As expected, different initializations of the updates in Equations (38) and (39) simply resulted in shifts of an otherwise pristine image in the reconstruction.

Figure 12. Reconstruction Results for Phasor Approach

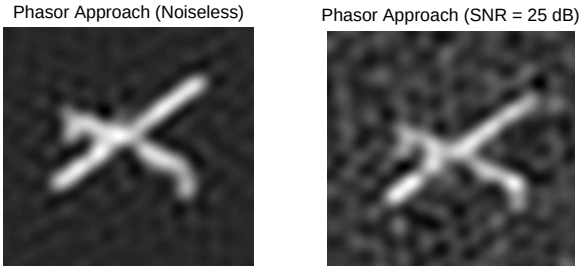

5 CONCLUSIONS

In this paper, we have examined the ambiguities caused by the 2π-periodicity of interferometric phase in Redundant Spacing Calibration. In particular we have described their fundamental presence in **existing RSC methods** whether the observables considered are the measured baseline phasors or their phases. **In the former, e.g. by Greenaway (1990), they are manifested as phase-wrapping errors, and in the latter, e.g. by Marthi & Chengalur (2014), as false minima. We have demonstrated that in either case, these ambiguities can result in noticeable distortion of the reconstructed image.**

Using the Closest-Vector-Problem formulation of the unwrapping problem due to Lannes & Anterrieu (1999), we have developed the notion of a wrap-invariant pattern. For wrap-invariant patterns, the impact of the 2π-periodicity can be completely eliminated (c.f. Section 2) using well-known algorithms from lattice theory and the Smith Normal Form, and reduced to a mere image shift (c.f. Section 4) when existing, fast approaches are used. Phase-approach solutions (Arnot et al. 1985), (Greenaway 1990), (Wieringa 1992), (Lannes & Anterrieu 1999)) are commonly used to quickly obtain an initial point to aid in the convergence of the Phasor approach. They are obtained by selecting specific solutions from the general family in Equation (24) via enforcement of additional constraints on the solution. Phasor approaches seek those complex gains and object visibilities which minimize a squared-residual with respect to the observed complex visibilities (Wijnholds & Noorishad 2012), (Liu et al. 2010), (Marthi & Chengalur 2014) using, for example, gradient-descent methods. We have seen that the same 2π-ambiguity which creates a family of Phase-approach solutions also produces a corresponding family of global minima in the Phasor approach. For either case, our results show that for wrap-invariant patterns, this family represents merely shifted versions of the true image. We have also extended this analysis to show that wrap-invariant patterns admit reliable imaging using standard, and generalized, phase closures. Conversely we show that patterns which are not wrap-invariant can suffer from distortion of the sort depicted in Figure 3.

The prognosis for mitigation of the ambiguity issues raised in this paper is quite positive. Random patterns appear to satisfy the wrap-invariance condition with high probability. Moreover, failure to meet this condition amounts to the existence of a particular kind of cycle in the interferometric graph which can be easily isolated; a chief contribution of this paper is a simple algorithm for identifying such cycles so that they can be removed by the array designer. Finally, we have shown an example execution of the algorithm to diagnose a member of a popular pattern which is not wrap-invariant. It is clear that with careful array design, both Phase- and Phasor-based RSC techniques can reliably produce quality image reconstructions free from discernible artifacts.

ACKNOWLEDGEMENTS

ACKNOWLEDGEMENT: This work is sponsored by the Assistant Secretary of Defense for Research and Engineering under Air Force Contract FA8721-05-C-0002. Opinions, interpretations, conclusions, and recommendations are those of the author and are not necessarily endorsed by the United States Government.

Binoy Kurien would like to acknowledge the MATLAB-based software package NUFFT (Fessler 2003) developed by Prof. Jeff Fessler and his students at the University of Michigan. This software was used to create the image reconstruction results shown in this paper. He would also like to acknowledge the MATLAB-based software packages *Variable Precision Integer Arithmetic* (D'Errico 2009) developed by John D'Errico, and the Smith Normal Form MATLAB package developed by John Gilbert (Gilbert 1999). This software was used to perform the arithmetic operations in the Smith Normal Form computations in the paper.

REFERENCES

Agrell E., Eriksson T., Vardy A., Zeger K., 2002, IEEE Transactions on Information Theory, 48, 2201

Ali Z. S., et al., 2015, The Astrophysical Journal, 809, 61

Arnot N., Atherton P., Greenaway A., Noordam J., 1985, Traitement du Signal, 2, 129

Babai L., 1986, Combinatorica, 6, 1

Besnerais G. L., Lacour S., Mugnier L. M., Thiébaut E., Perrin G., Meimon S., 2008, IEEE Journal of Selected Topics in Signal Processing, 2, 767

Blanchard P., Greenaway A., Anderton R., Appleby R., 1996, J. Opt. Soc. Am. A, 13, 1593

Bretscher O., 2001, Linear Algebra with Applications, 2nd edn. Prentice Hall, Upper Saddle River, New Jersey, USA

D'Errico J., 2009, Variable Precision Integer Arithmetic, http://www.mathworks.com/matlabcentral/fileexchange/22725-variable-precision-integer-arithmetic

Eastwood R., Johnson A., Greenaway A., 2009, J. Opt. Soc. Am. A., 26, 195

Fessler J., 2003, NUFFT MATLAB Toolbox, http://web.eecs.umich.edu/~fessler/code/

Gilbert J., 1999, Smith Normal Form of an Integer Matrix, http://www.mathworks.com/matlabcentral/newsreader/view_thread/13728

Glindemann A., 2011, Principles of Stellar Interferometry, 1st edn. Springer, New York, USA

Greenaway A. H., 1990, Proc. SPIE 1351, Digital Image Synthesis and Inverse Optics, 1351, 738

Greenaway A., 1994, in NATO ASI Series. Series C: Mathematical and Physical Sciences, Vol. 423, Adaptive Optics for Astronomy. Kluwer Academic Publishers, Boston, USA

Labeyrie A., Lipson S., Nisenson P., 2006, An Introduction to Optical Stellar Interferometry, 1st edn. Cambridge University Press, New York, NY

Lacour S., Thiébaut E., Perrin G., 2007, Monthly Notices of the Royal Astronomical Society, 374, 832

Lannes A., 2003, in , Vol. 126, Advances in Imaging and Electron Physics. Academic Press, Boston, USA

Lannes A., Anterrieu E., 1999, Journal of the Optical Society of America A, 16, 2866

Liu A., Tegmark M., Morrison S., Lutomirski A., Zaldarriaga M., 2010, Monthly Notices of the Royal Astronomical Society, 408, 1029

Liu L., He Y., Zhang J., Jia H., Ma J., 2014, Optical Engineering, 53, 1

Marthi V. R., Chengalur J., 2014, Monthly Notices of the Royal Astronomical Society, 437, 524
Martinache F., 2010, The Astrophysical Journal, 724, 464
Newman M., 1972, Integral Matrices, 1st edn. Academic Press, New York, NY
Perrin G., Lacour S., Woillez J., Thiebaut E., 2006, Monthly Notices of the Royal Astronomical Society, 373, 747
Readhead A., Nakajima T., Pearson T., Neugebauer G., Oke J., Sargent W., 1988, Astronomical Journal, 95, 1278
Smith H., 1861, Phil. Trans R. Soc. Lond., 151, 293
Thiébaut E., 2013, New Concepts in Imaging: Optical and Statistical Models, 59, 157
Wieringa M., 1992, Experimental Astronomy, 2, 203
Wijnholds S., Noorishad P., 2012, in Signal Processing Conference (EUSIPCO), 2012 Proceedings of the 20th European. pp 1304–1308
Zheng H., Tegmark M., Buza V., Dillon J., 2014, Monthly Notices of the Royal Astronomical Society, 445, 1084

APPENDIX A: PROOF OF LEMMA 4.2

In this section, we prove Lemma 4.2, which states the following:

Given wrap-invariance, the (column) vector $\mathbf{U_X M}_K^+ \boldsymbol{e}_h^*$ *has integer entries below row 2.*

Given that we have a wrap-invariant pattern, we know that the elementary divisors of $\mathbf{M}$ are all 1. Hence there exists an integer vector $\boldsymbol{k}_0$ such that:

$$\boldsymbol{e}_h^* = \mathbf{M}\boldsymbol{k}_0 \tag{A1}$$

Substituting Equations (A1) and (25) into Equation (26), we obtain:

$$\boldsymbol{e}_\sigma = \mathbf{V}_\sigma \Sigma_\sigma^+ \mathbf{U}_\sigma^T \mathbf{U}_\sigma \Sigma_\sigma \mathbf{V}_\sigma^T \boldsymbol{k}_0 \tag{A2}$$

Noting that $\mathbf{U}_\sigma$ is orthogonal, this equation can be simplified to

$$\boldsymbol{e}_\sigma = (\mathbf{V}_\sigma - \mathbf{N})\mathbf{V}_\sigma^T \boldsymbol{k}_0 \tag{A3}$$

where $\mathbf{N}$ is a matrix of the same size as $\mathbf{V}_\sigma$, which is zero except for the last three columns. These last three columns are identical to those of $\mathbf{V}_\sigma$, and hence by Lemma 4.1 comprise an orthogonal basis for the nullspace of $\mathbf{M}$. Noting the orthogonality of $\mathbf{V}_\sigma$, this can be further simplified to:

$$\boldsymbol{e}_\sigma = \boldsymbol{k}_0 - \mathbf{N}\mathbf{V}_\sigma^T \boldsymbol{k}_0 \tag{A4}$$

To proceed, the following Definition will be useful:

Definition A.1 (The canonical basis for the nullspace of M): The canonical basis $\{\boldsymbol{w}_i\}, i \in 1, 2, 3$ for the three-dimensional nullspace of $\mathbf{M}$ can be derived trivially from the well-known tilt-position degeneracy in interferometry described in Section 2.1.1 (Wieringa 1992). Namely, we can define the basis as the columns of a $(N + d) \times 3$ matrix $\mathbf{W}_{ker(\mathbf{M})}$ as follows:

$$\mathbf{W}_{ker(\mathbf{M})} = \{\boldsymbol{w}_1 | \boldsymbol{w}_2 | \boldsymbol{w}_3\} = \begin{bmatrix} \mathbb{1}_{N\times 1} & \boldsymbol{r}_x & \boldsymbol{r}_y \\ \boldsymbol{0} & \Delta\boldsymbol{r}_x & \Delta\boldsymbol{r}_y \end{bmatrix} \tag{A5}$$

where $\boldsymbol{r}_x$ and $\boldsymbol{r}_y$ are the $x-$ and $y-$positional coordinates of the apertures associated with each row, respectively, and $\Delta\boldsymbol{r}_x$ and $\Delta\boldsymbol{r}_y$ their respective pairwise differences. □

Note that each of the three non-zero column vectors $\{\boldsymbol{v}_k\}, k \in 1, 2, 3$ in $\mathbf{N}$ can be expressed as a linear combinations of the elements of the canonical basis $\{\boldsymbol{w}_i\}, i \in 1, 2, 3$ defined above, i.e.

$$\boldsymbol{v}_k = a_1\boldsymbol{w}_1 + a_2\boldsymbol{w}_2 + a_3\boldsymbol{w}_3 \tag{A6}$$

As in Section 4, let us again use K to denote the set of indices in $\boldsymbol{e}_\sigma$ associated with the Fourier phases (as opposed to the piston phases), and their corresponding rows in $\mathbf{N}$. Hence we have:

$$\mathbf{U_X}\boldsymbol{e}_{\sigma,K} = \mathbf{U_X}\boldsymbol{k}_{0,K} - \mathbf{U_X}\mathbf{N}_K\mathbf{V}_\sigma^T\boldsymbol{k}_0 \tag{A7}$$

Since $\mathbf{U_X}$ is an integer matrix, the first term is clearly integral. Let us then examine the second term, and in particular, the product $\mathbf{U_X N}_K$. By substitution from Equation (A6), we see that or any of the three non-zero columns $\boldsymbol{v}_{K,k}$ of $\mathbf{N}_K$, we have:

$$\mathbf{U_X}\boldsymbol{v}_{K,k} = a_1\mathbf{U_X}\boldsymbol{w}_{1,K} + a_2\mathbf{U_X}\boldsymbol{w}_{2,K} + a_3\mathbf{U_X}\boldsymbol{w}_{3,K} \tag{A8}$$

where $\{\boldsymbol{w}_{j,K}\}$ are the vectors comprising the lower partition of Equation (A5). The first term in Equation (A8) is trivially $\boldsymbol{0}$ since that $\boldsymbol{w}_{1,J}$ is the zero-vector. Now recall that $\mathbf{U}_X$ is a matrix which annihilates all the spatial frequencies in the matrix $\mathbf{X}$ below row 2. But from Definition A.1, these spatial frequencies are identically the contents of the two columns $\boldsymbol{w}_{2,K}$ and $\boldsymbol{w}_{3,K}$ (up to a uniform scaling factor). Therefore the column vector in Equation (A8) is zero below row 2. This means in turn that the second term in Equation (A7) is zero below row 2, and hence that $\mathbf{U_X}\boldsymbol{e}_{\sigma,J}$ is integral below row 2 (since the first term is integral). □

This paper has been typeset from a TEX/LATEX file prepared by the author.